Supplement of Biogeosciences, 22, 4601–4626, 2025
https://doi.org/10.5194/bg-22-4601-2025-supplement

Biogeosciences Open Access EGU

Supplement of

Bio-climatic factors drive spectral vegetation changes in Greenland

Tiago Silva et al.

Correspondence to: Tiago Silva (tiago.ferreira-da-silva@uni-graz.at)

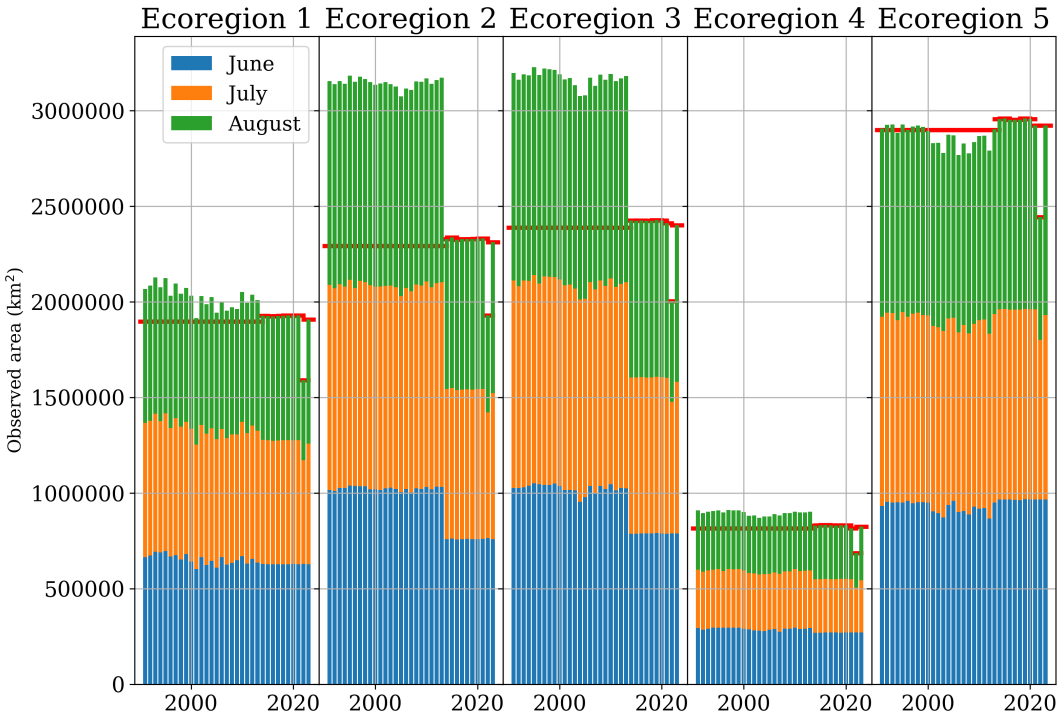

Figure S1. Monthly area extent (#observations×area) cover by AVHRR and VIIRS between 1991 and 2023 as dependent on ecoregion. The red line marks the averaged monthly area extent based on the period 2014–2023.

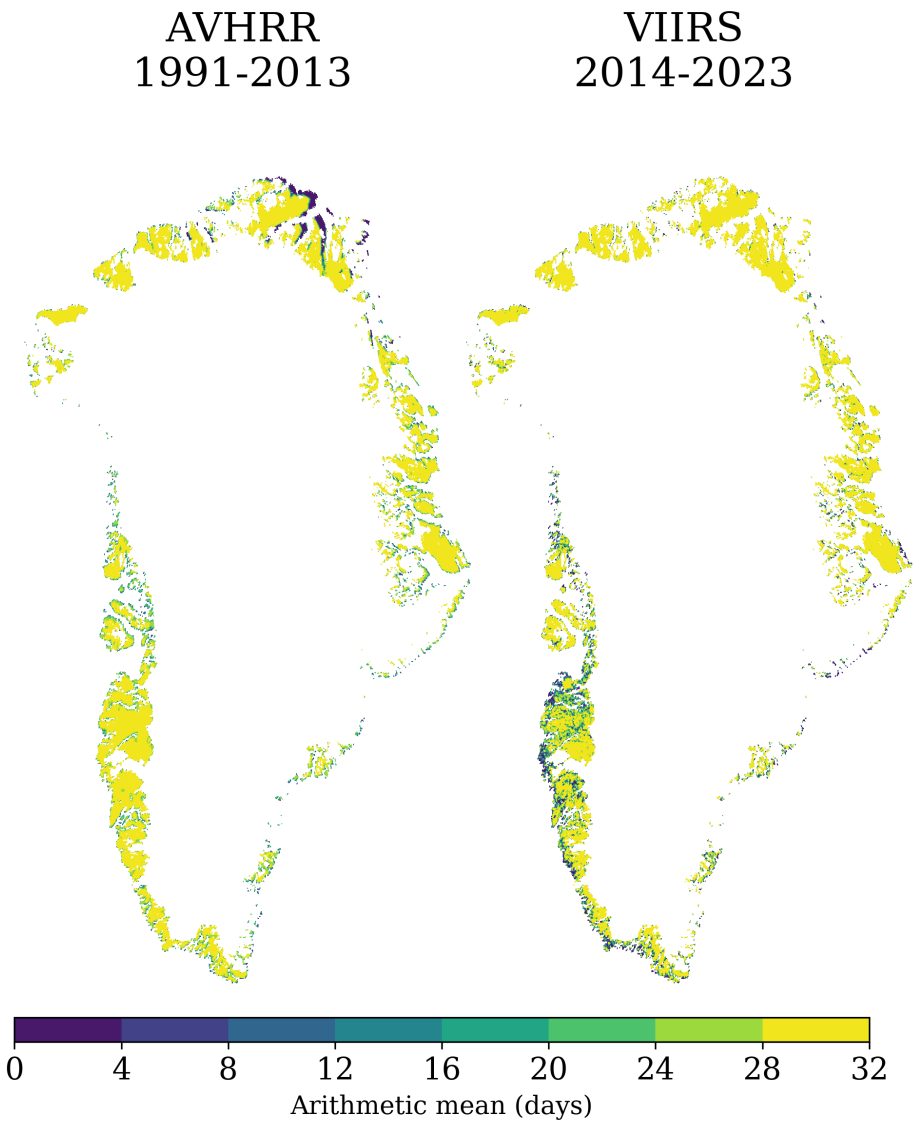

Figure S2. Arithmetic mean of the monthly number observation during summer for AVHRR and VIIRS period before the n adjustment.

Figure S3. Standard deviation of the monthly number observation during summer for AVHRR and VIIRS period before the n adjustment.

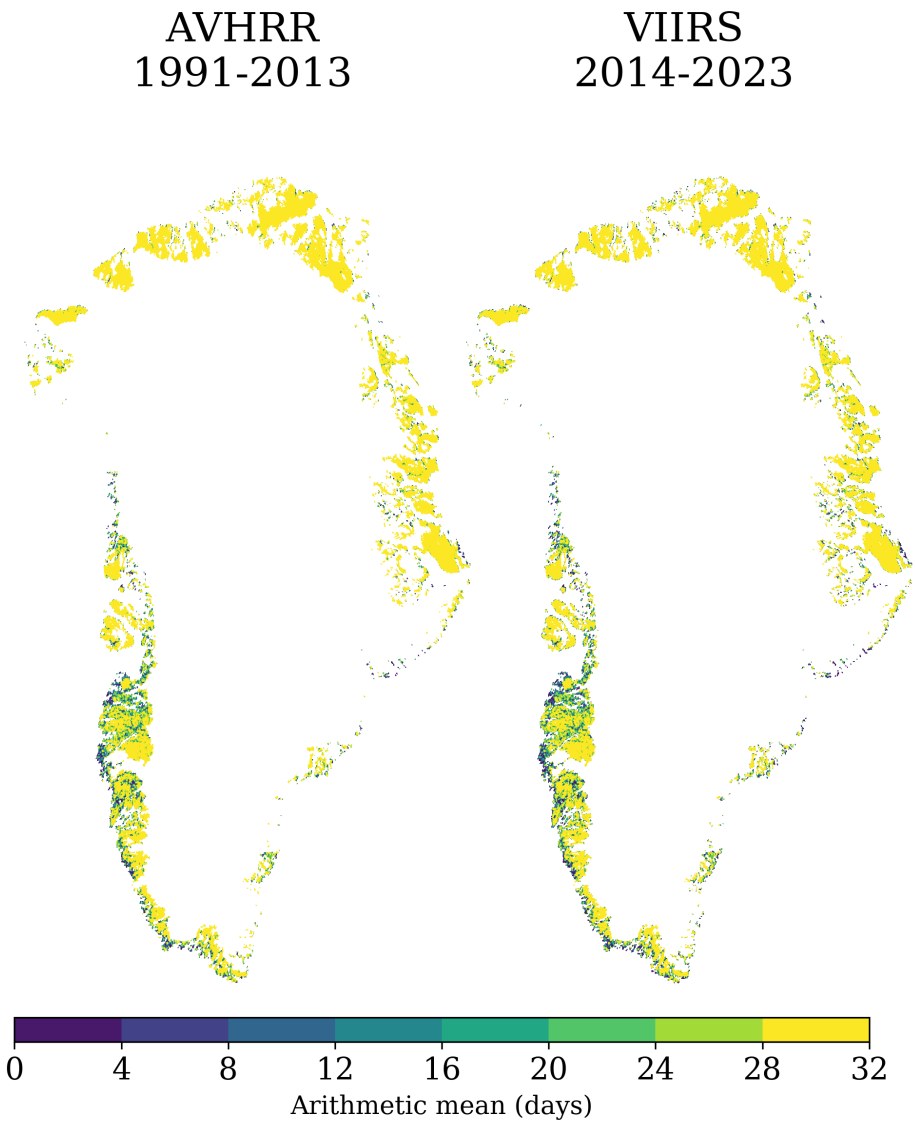

Figure S4. Arithmetic mean of the monthly number observation during summer for AVHRR and VIIRS period after the n adjustment.

Figure S5. Arithmetic mean of the monthly number observation during summer for AVHRR and VIIRS period after the n adjustment.

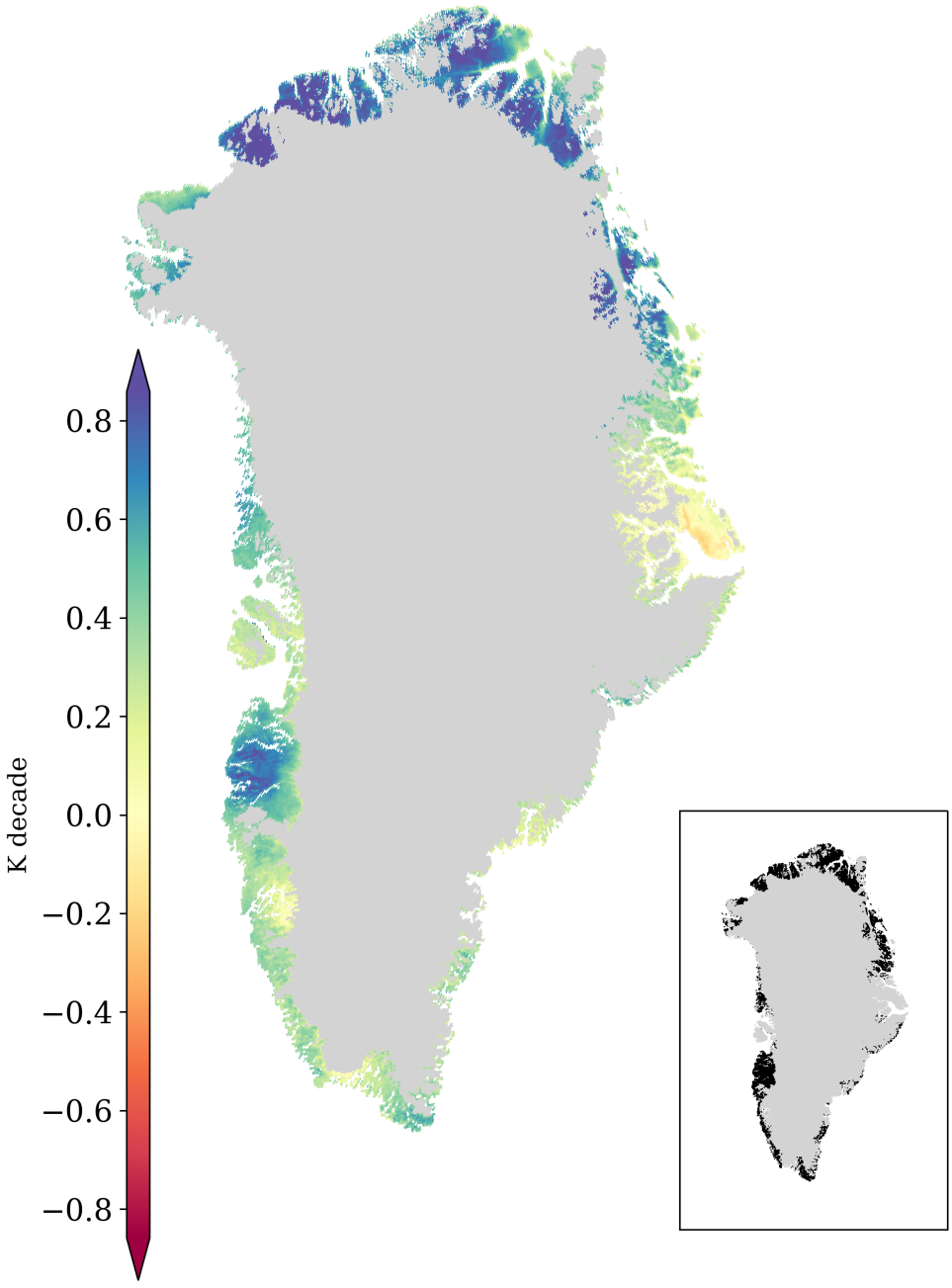

Figure S6. 2-m air-temperature trends in summer across ice-free Greenland from CARRA between 1991 and 2023. Significant confidence levels higher than 95%, with the null hypothesis that the slope is equal to zero, are shaded in the map in the lower right corner.

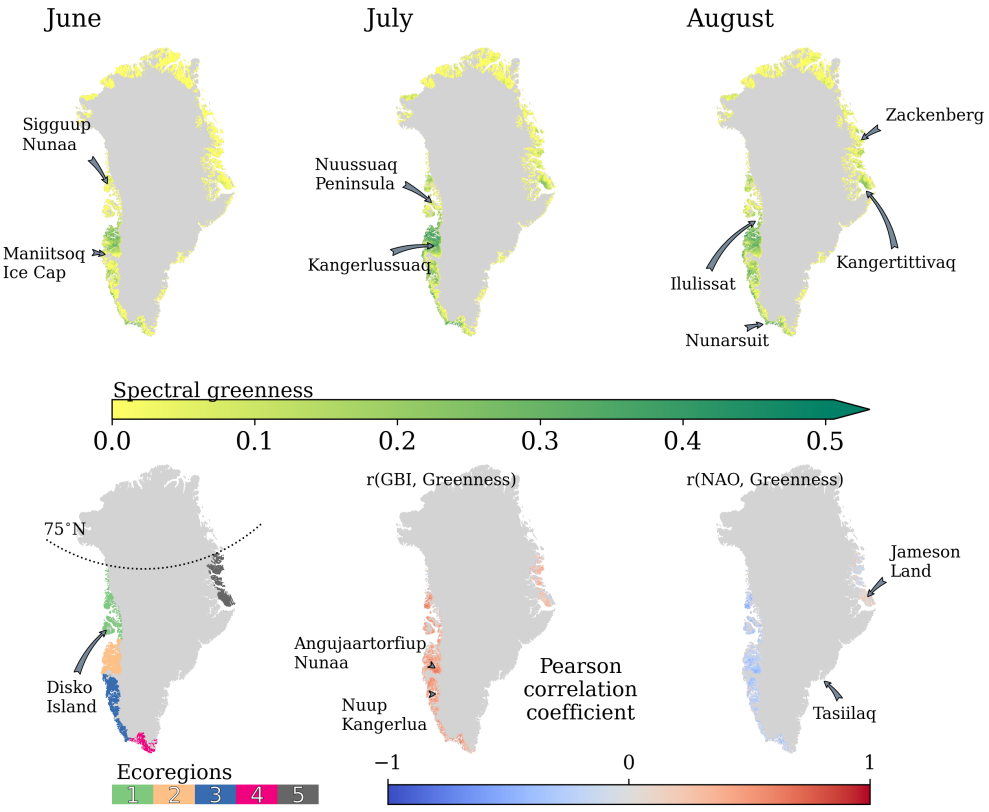

Figure S7. Averaged spectral greenness (based on the period 1991-2023) for June, July and August (upper panel). No scale shown in the colour bar because the aim is to illustrate spectral greenness patterns, not absolute values; ecoregions in ice-free Greenland (lower left panel); Pearson correlation coefficient between the summer averaged vegetation and the Greenland Blocking Index (GBI, lower central panel), and the North Atlantic Oscillation (NAO, lower right panel). Placenames referenced in the study are displayed.

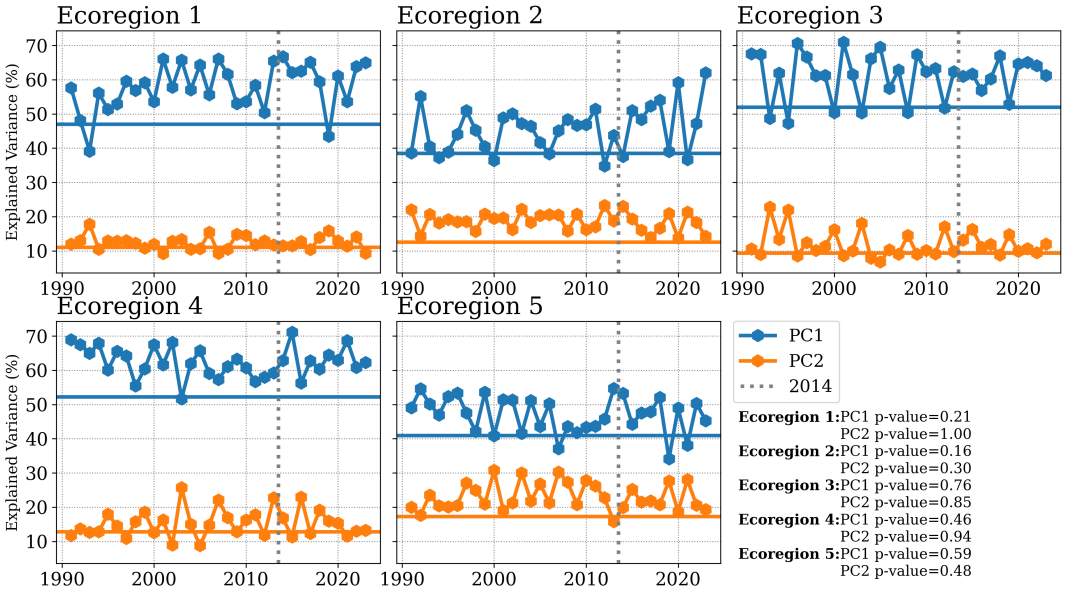

Figure S8. Interannual explained variance for the first and the second principal component across ecoregions between 1991 and 2023. The explained variance of the combined period is shown as horizontal continuous line. The vertical dash line marks the change of satellite in 2014.

Table S1. Correlation coefficient between green vegetation extent and the Greenland Blocking Index and its corresponding p-value (r, p-value) during three periods: AVHRR (1991-2013), VIIRS (2014-2023) and full period for each ecoregion.

Ecoregion	Period	June	July	August	JJA
1	1991-2013	(0.4,0.1)	(0.5,0.02)	(0.3,0.25)	(0.6,$p < 0.01$)
	2014-2023	(0.4,0.31)	(0.8,0.02)	(0.5,0.14)	(0.8,0.02)
	1991-2023	(0.4,0.03)	(0.5,$p < 0.01$)	(0.4,0.04)	(0.6,$p < 0.01$)
2	1991-2013	(0.4,0.06)	(0.5,0.01)	(0.4,0.05)	(0.6,$p < 0.01$)
	2014-2023	(0.5,0.19)	(0.5,0.14)	(0.5,0.19)	(0.8,0.01)
	1991-2023	(0.4,0.01)	(0.5,$p < 0.01$)	(0.4,0.04)	(0.6,$p < 0.01$)
3	1991-2013	(0.3,0.22)	(0.3,0.13)	(0.5,$p < 0.01$)	(0.5,0.02)
	2014-2023	(0.7,0.02)	(0.4,0.31)	(0.4,0.22)	(0.8,0.02)
	1991-2023	(0.4,0.01)	(0.4,0.03)	(0.5,$p < 0.01$)	(0.5,$p < 0.01$)
4	1991-2013	(0.4,0.04)	(0.4,0.09)	(0.1,0.54)	(0.6,$p < 0.01$)
	2014-2023	(0.6,0.1)	(0.4,0.22)	(0.5,0.14)	(0.8,0.02)
	1991-2023	(0.4,0.01)	(0.4,0.02)	(0.3,0.06)	(0.6,$p < 0.01$)
5	1991-2013	(0.0,0.9)	(0.1,0.51)	(0.5,0.03)	(0.2,0.46)
	2014-2023	(0.4,0.25)	(0.0,1.0)	(0.5,0.19)	(0.4,0.31)
	1991-2023	(0.1,0.57)	(0.2,0.31)	(0.5,$p < 0.01$)	(0.2,0.28)

Table S2. Monthly trends in percentage per decade and its corresponding p-value (slope, p-value) for green vegetation extent during three periods: AVHRR (1991-2013), VIIRS (2014-2023) and full period for each ecoregion. The trend corresponds to the T-S slope and the p-value to the Hamed and Rao Modified M-K test.

Ecoregion	Period	June	July	August	JJA
1	1991-2013	(0.4,0.33)	(2.58,0.14)	(2.17,0.01)	(1.52,0.02)
	2014-2023	(-1.82,0.47)	(-36.3,0.03)	(-11.79,0.22)	(-27.32,0.05)
	1991-2023	(0.07,0.85)	(3.67,0.01)	(6.35,p < 0.01)	(2.0,0.02)
2	1991-2013	(6.15,0.32)	(3.13,0.03)	(13.89,p < 0.01)	(8.12,0.03)
	2014-2023	(-33.91,0.21)	(-22.63,p < 0.01)	(-12.05,0.21)	(-34.89,0.02)
	1991-2023	(2.52,0.7)	(1.83,0.25)	(8.71,p < 0.01)	(4.8,0.04)
3	1991-2013	(3.01,0.1)	(4.72,0.2)	(7.6,p < 0.01)	(4.74,0.02)
	2014-2023	(-14.71,0.37)	(-33.15,0.01)	(-22.14,0.02)	(-28.4,0.11)
	1991-2023	(-0.04,1.0)	(2.82,0.21)	(7.46,p < 0.01)	(3.2,0.14)
4	1991-2013	(3.73,0.03)	(2.23,0.29)	(3.2,0.21)	(3.42,0.02)
	2014-2023	(-0.27,1.0)	(-6.24,0.72)	(-5.87,1.0)	(-2.53,0.59)
	1991-2023	(3.81,p < 0.01)	(5.25,p < 0.01)	(7.67,p < 0.01)	(5.93,p < 0.01)
5	1991-2013	(0.03,p < 0.01)	(5.28,0.01)	(2.44,0.29)	(1.94,0.02)
	2014-2023	(-0.07,0.65)	(9.9,p < 0.01)	(16.62,0.37)	(9.32,0.37)
	1991-2023	(0.02,0.45)	(5.61,p < 0.01)	(8.1,p < 0.01)	(4.21,p < 0.01)

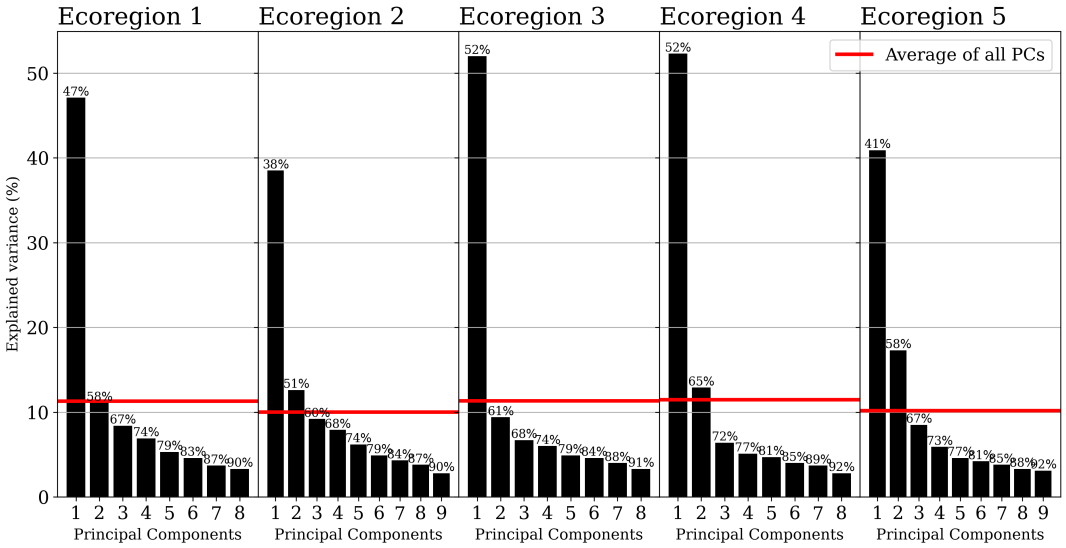

Figure S9. Explained variance among principal components and across ecoregions between 1991 and 2023 accounting for at least 90% of the variability among the 16 bioclimatic indicators. The averaged explained variance for the principal components accounting for at least 90% of the variability among the 16 bioclimatic indicators is drawn in red.

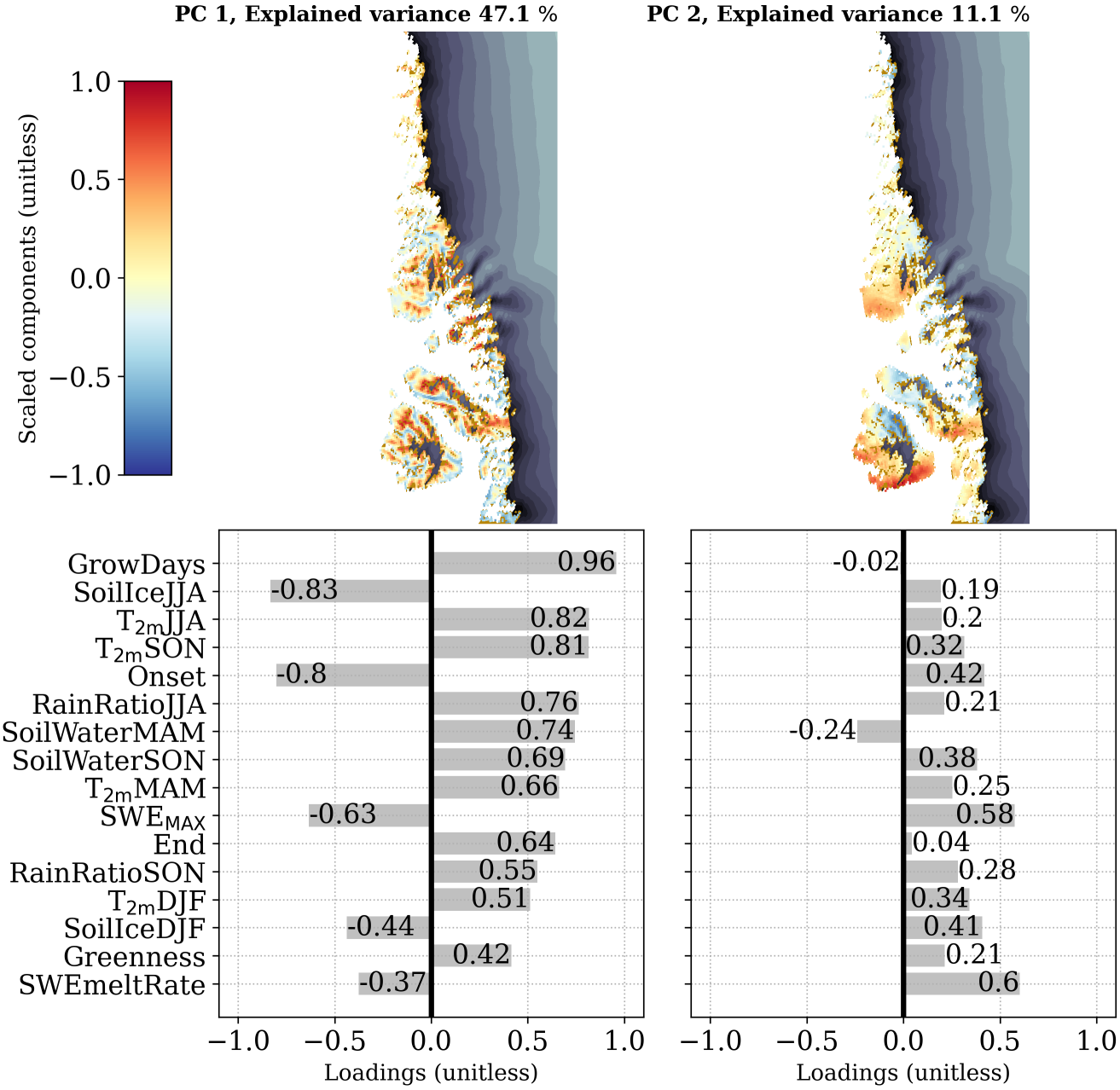

Figure S10. Spatial pattern of the averaged 1991–2023 scores for the first (PC1) and second (PC2) principal components in ecoregion 1, as well as the corresponding loadings of each component.

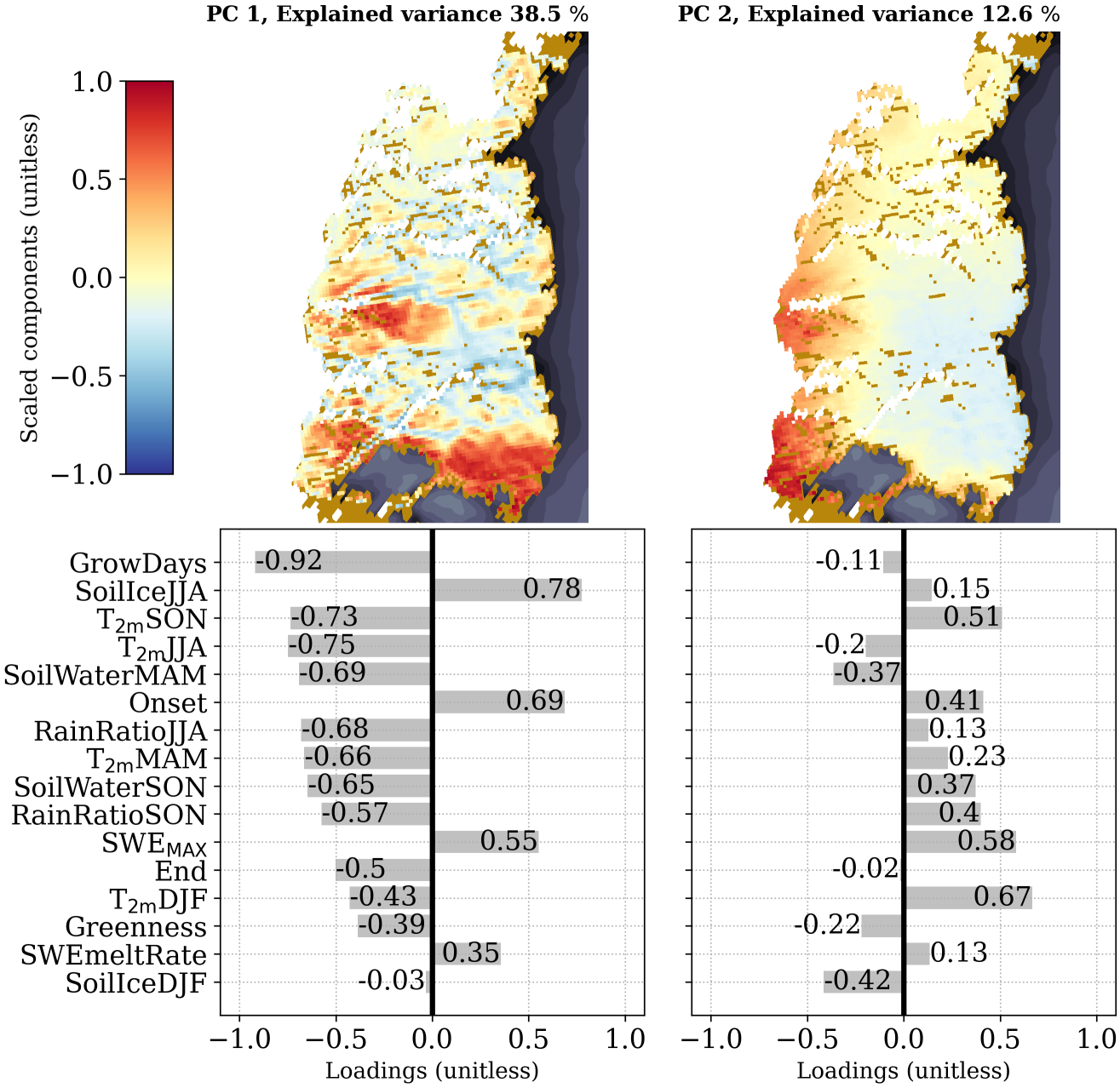

Figure S11. Spatial pattern of the averaged 1991–2023 scores for the first (PC1) and second (PC2) principal components in ecoregion 2, as well as the corresponding loadings of each component.

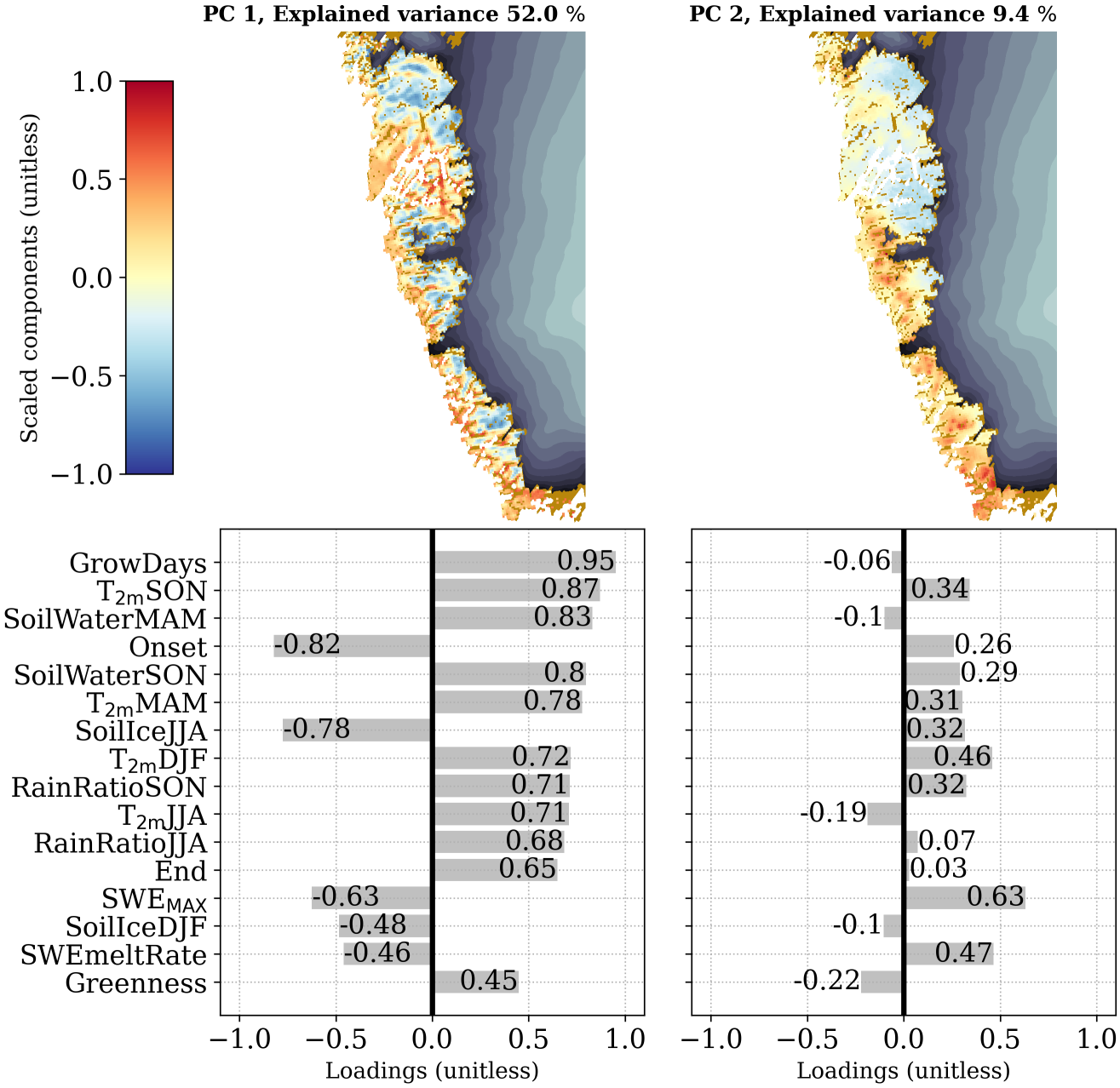

Figure S12. Spatial pattern of the averaged 1991–2023 scores for the first (PC1) and second (PC2) principal components in ecoregion 3, as well as the corresponding loadings of each component.

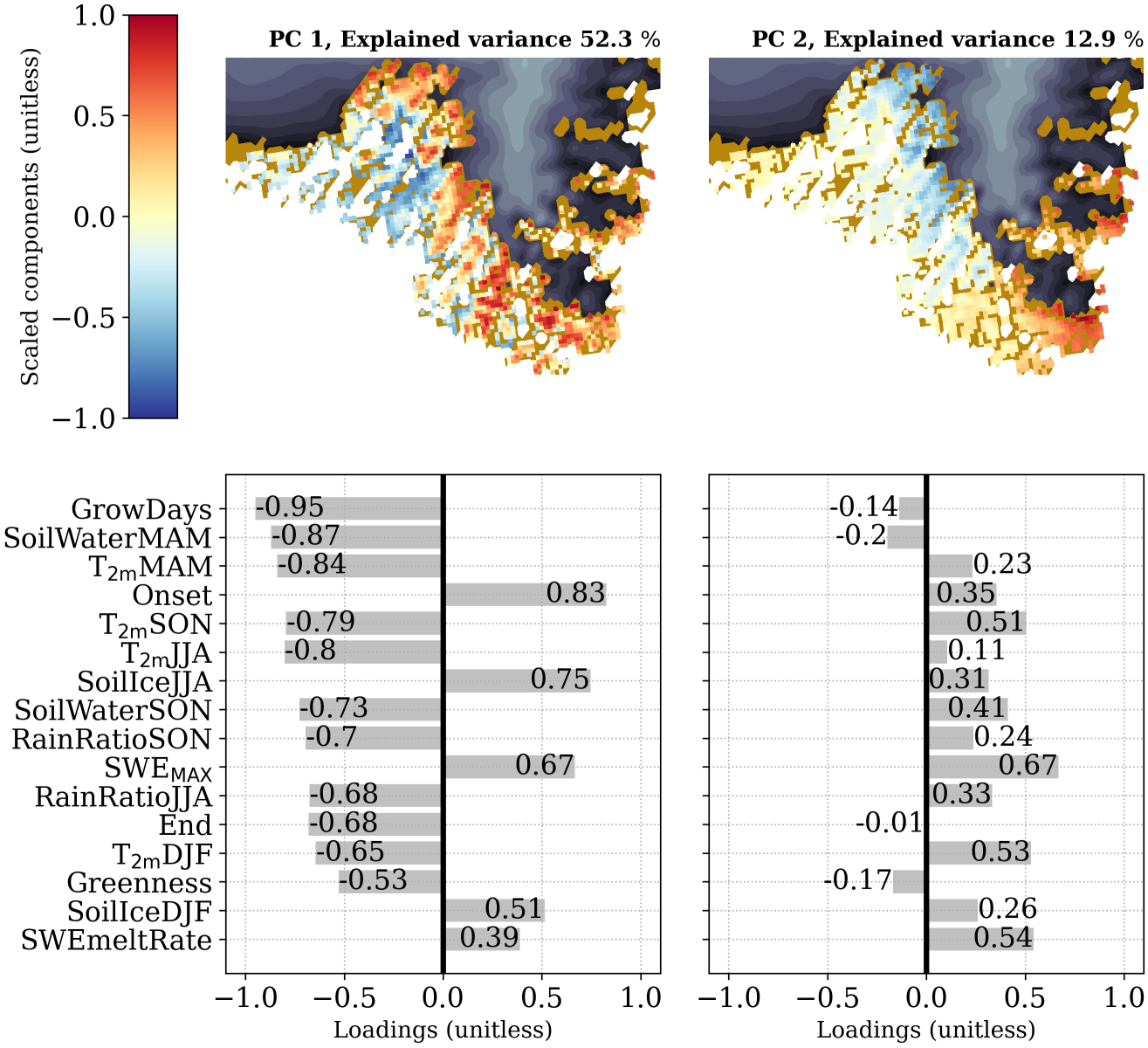

Figure S13. Spatial pattern of the averaged 1991–2023 scores for the first (PC1) and second (PC2) principal components in ecoregion 4, as well as the corresponding loadings of each component.

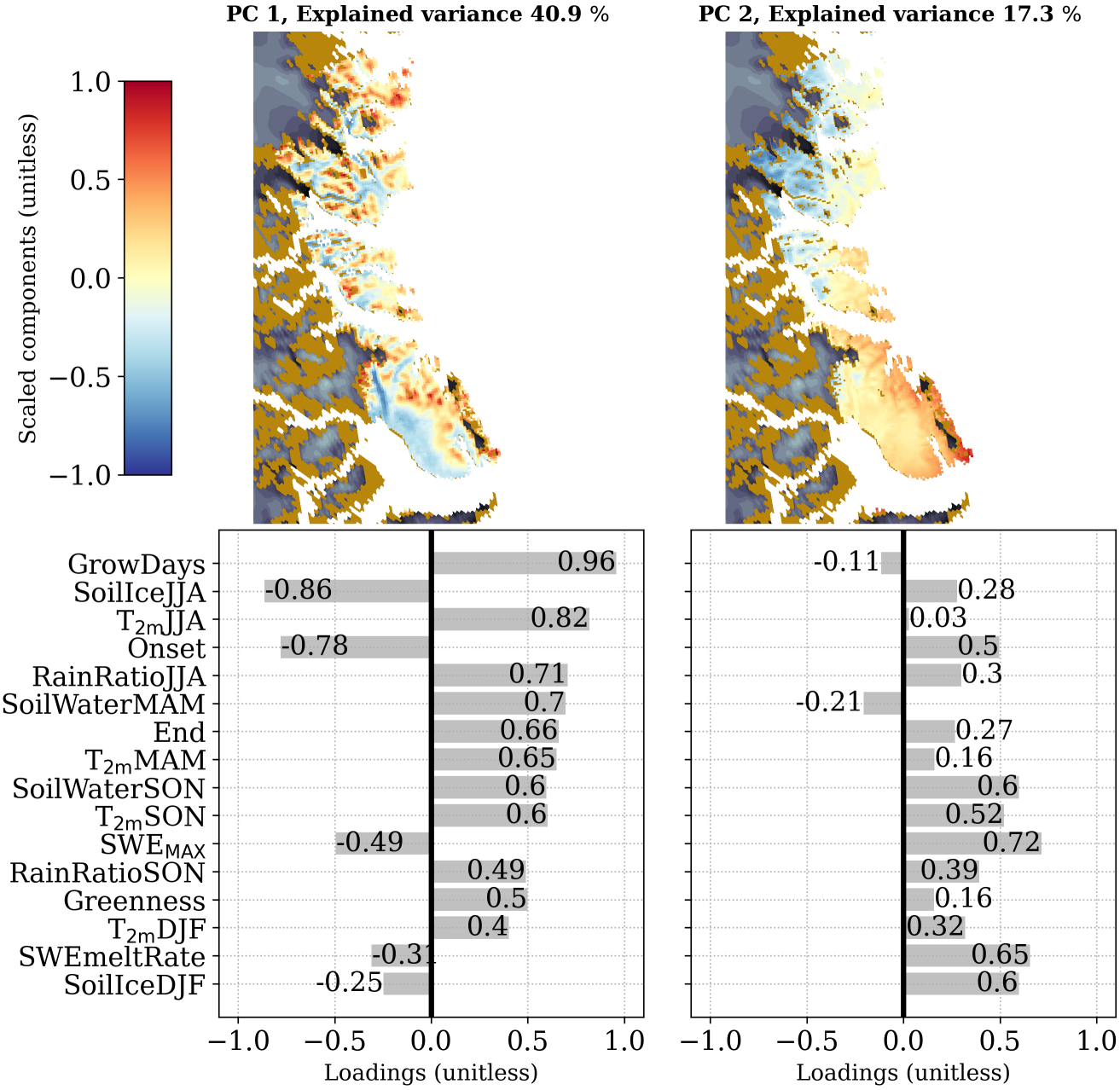

Figure S14. Spatial pattern of the averaged 1991–2023 scores for the first (PC1) and second (PC2) principal components in ecoregion 5, as well as the corresponding loadings of each component.

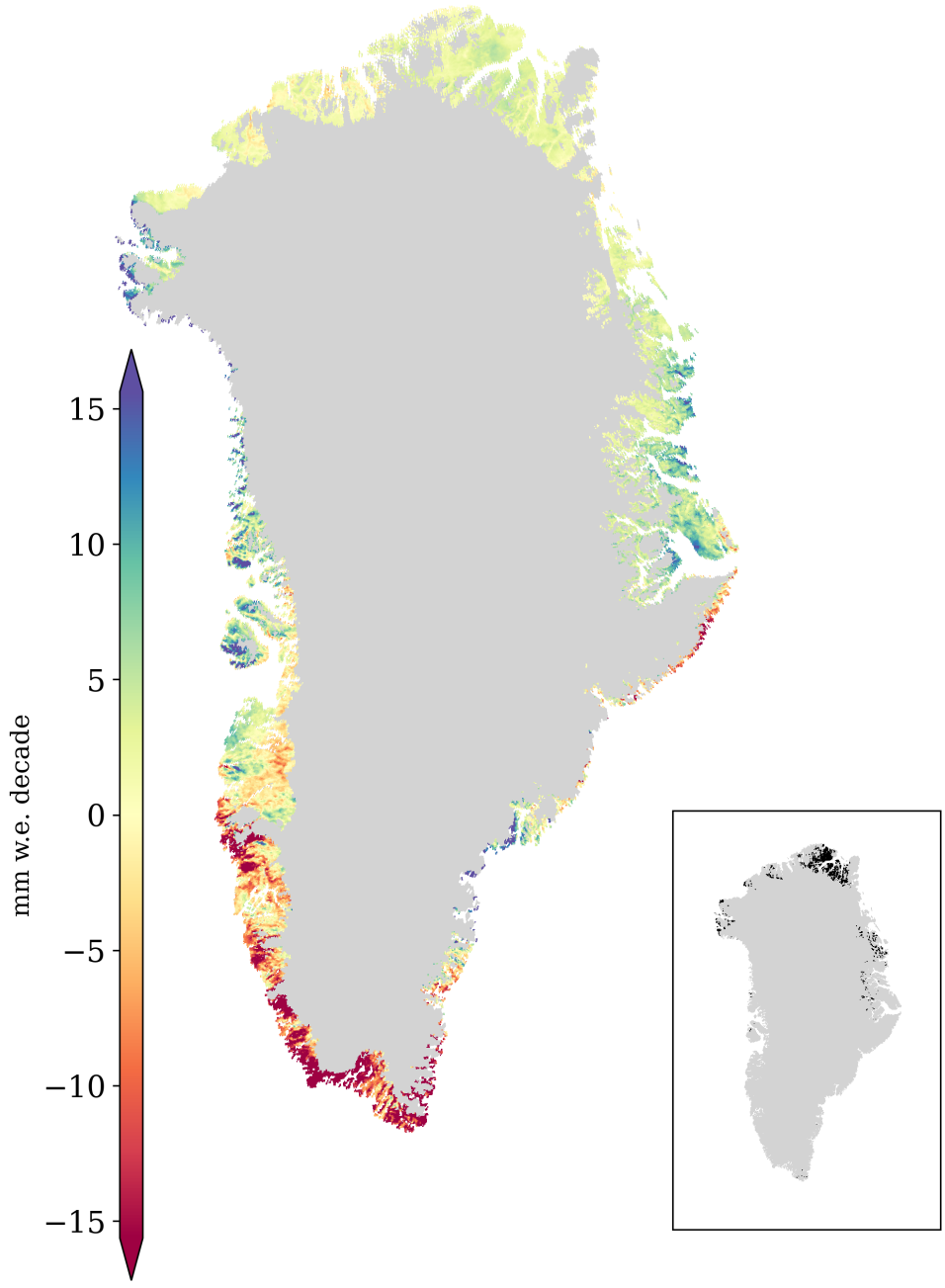

Figure S15. Total liquid precipitation trends in summer across ice-free Greenland from CARRA between 1991 and 2023. Significant confidence levels higher than 95%, with the null hypothesis that the slope is equal to zero, are shaded in the map in the lower right corner.

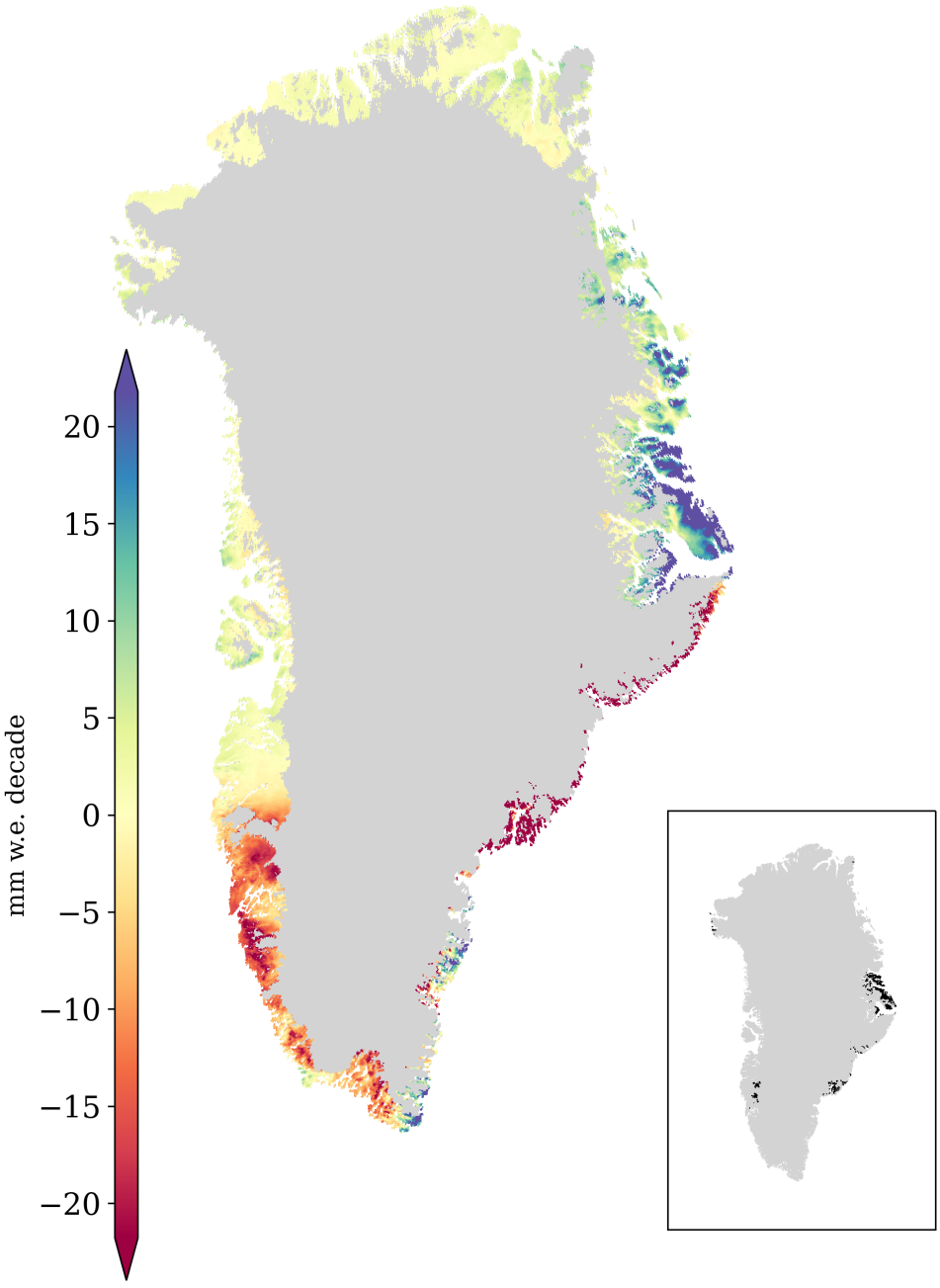

Figure S16. Total solid precipitation trends in winter across ice-free Greenland from CARRA between 1991 and 2023. Significant confidence levels higher than 95%, with the null hypothesis that the slope is equal to zero, are shaded in the map in the lower right corner.

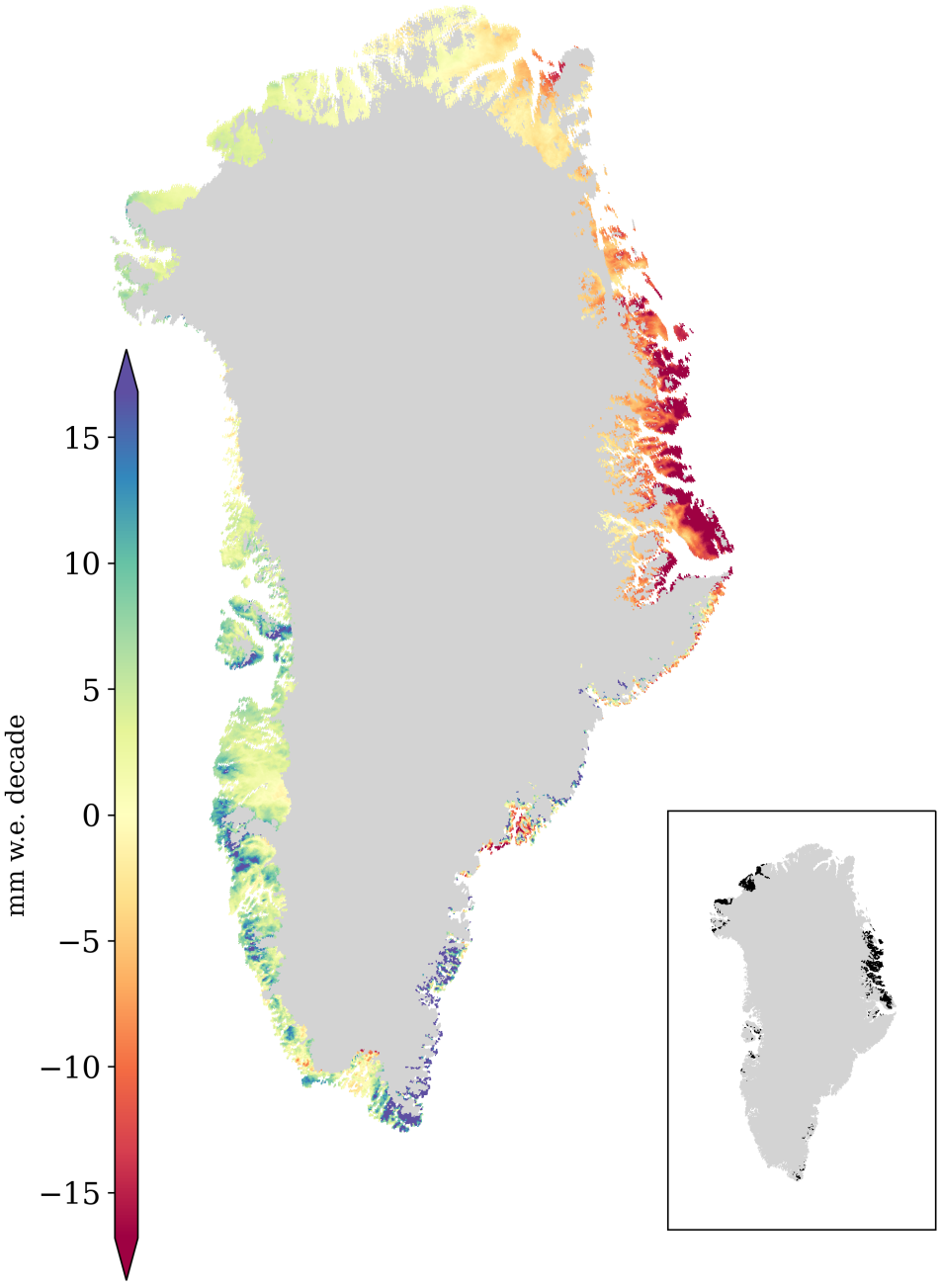

Figure S17. Total solid precipitation trends in spring across ice-free Greenland from CARRA between 1991 and 2023. Significant confidence levels higher than 95%, with the null hypothesis that the slope is equal to zero, are shaded in the map in the lower right corner.

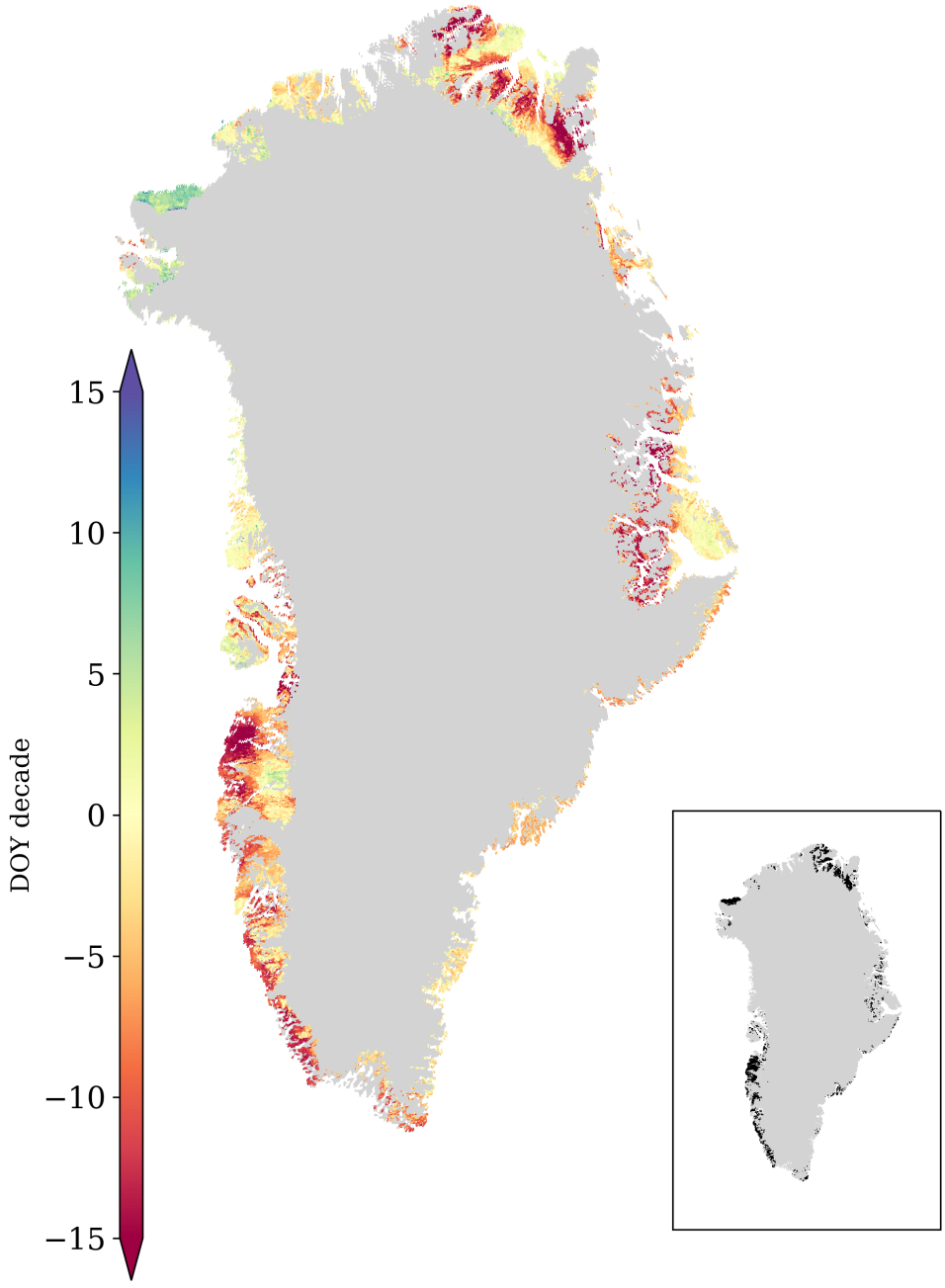

Figure S18. Trends for the day of the year with maximum snow water equivalent across ice-free Greenland from CARRA between 1991 and 2023. Significant confidence levels higher than 95%, with the null hypothesis that the slope is equal to zero, are shaded in the map in the lower right corner.

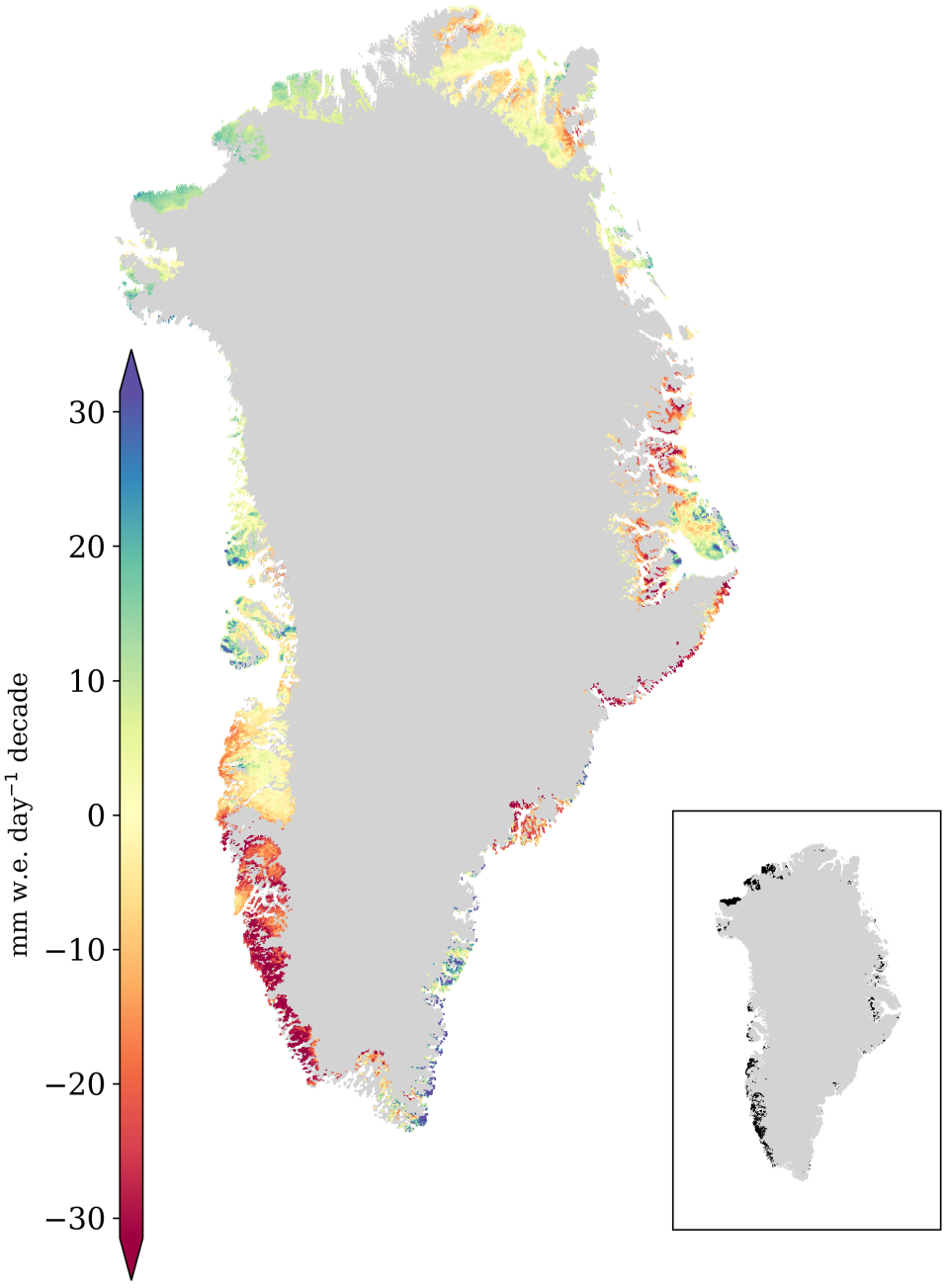

Figure S19. Trends for the snow water equivalent melt rate across ice-free Greenland from CARRA between 1991 and 2023. Significant confidence levels higher than 95%, with the null hypothesis that the slope is equal to zero, are shaded in the map in the lower right corner.

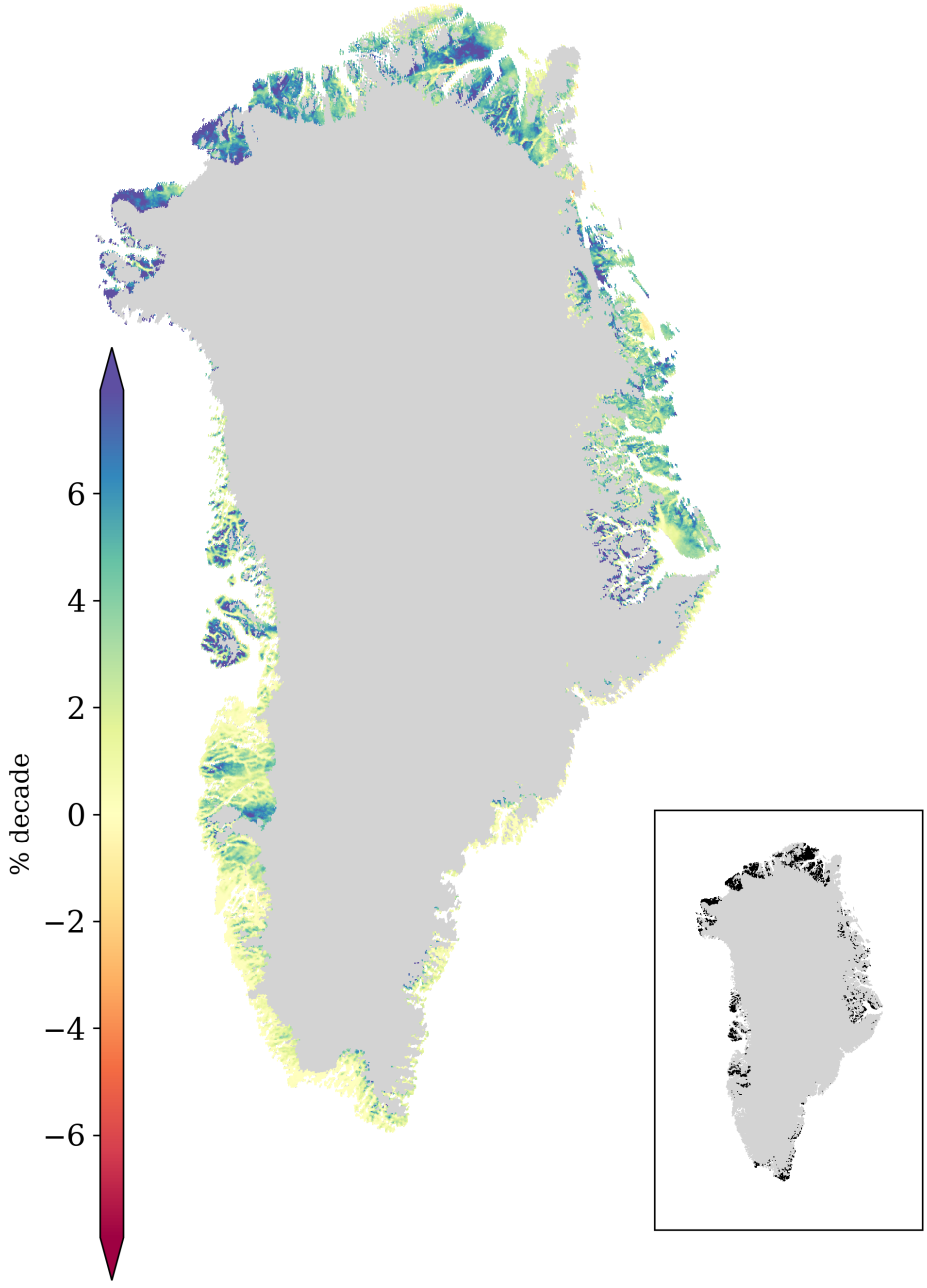

Figure S20. Trends for the rain ratio in summer across ice-free Greenland from CARRA between 1991 and 2023. Significant confidence levels higher than 95%, with the null hypothesis that the slope is equal to zero, are shaded in the map in the lower right corner.

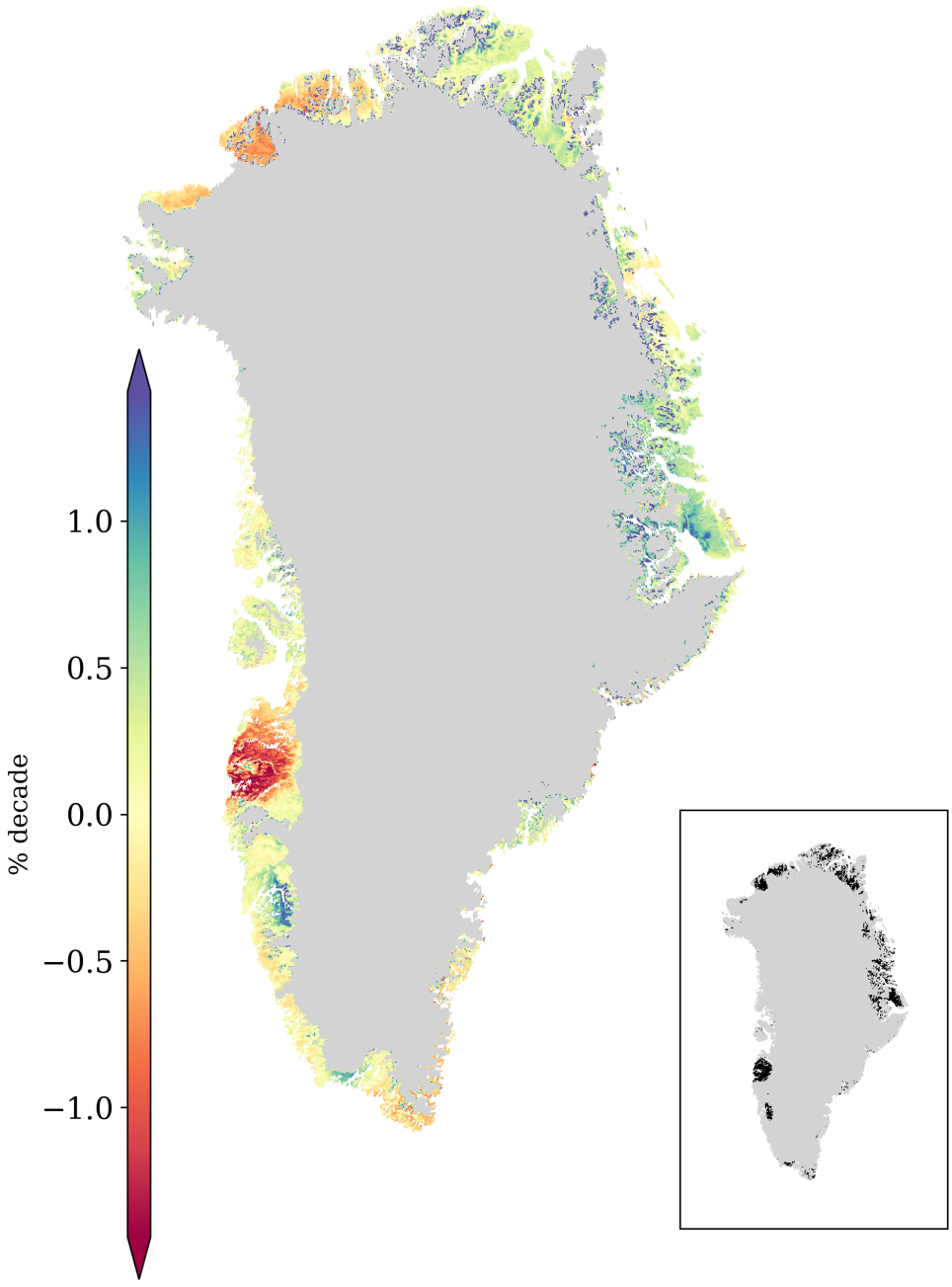

Figure S21. Trends in volumetric soil water in summer across ice-free Greenland from CARRA between 1991 and 2023. Significant confidence levels higher than 95%, with the null hypothesis that the slope is equal to zero, are shaded in the map in the lower right corner.

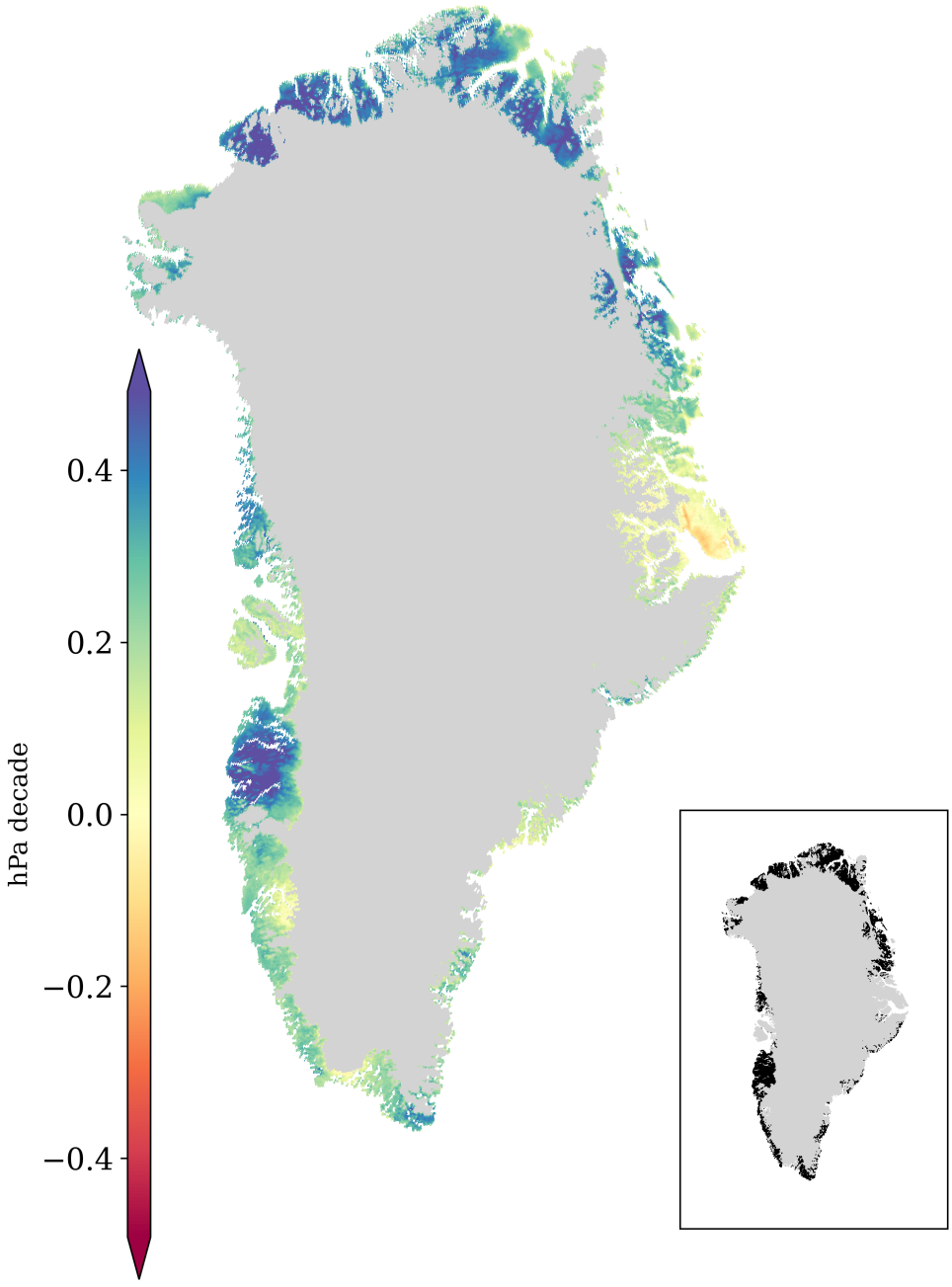

Figure S22. Trends in vapour pressure deficit in summer across ice-free Greenland from CARRA between 1991 and 2023. Significant confidence levels higher than 95%, with the null hypothesis that the slope is equal to zero, are shaded in the map in the lower right corner.

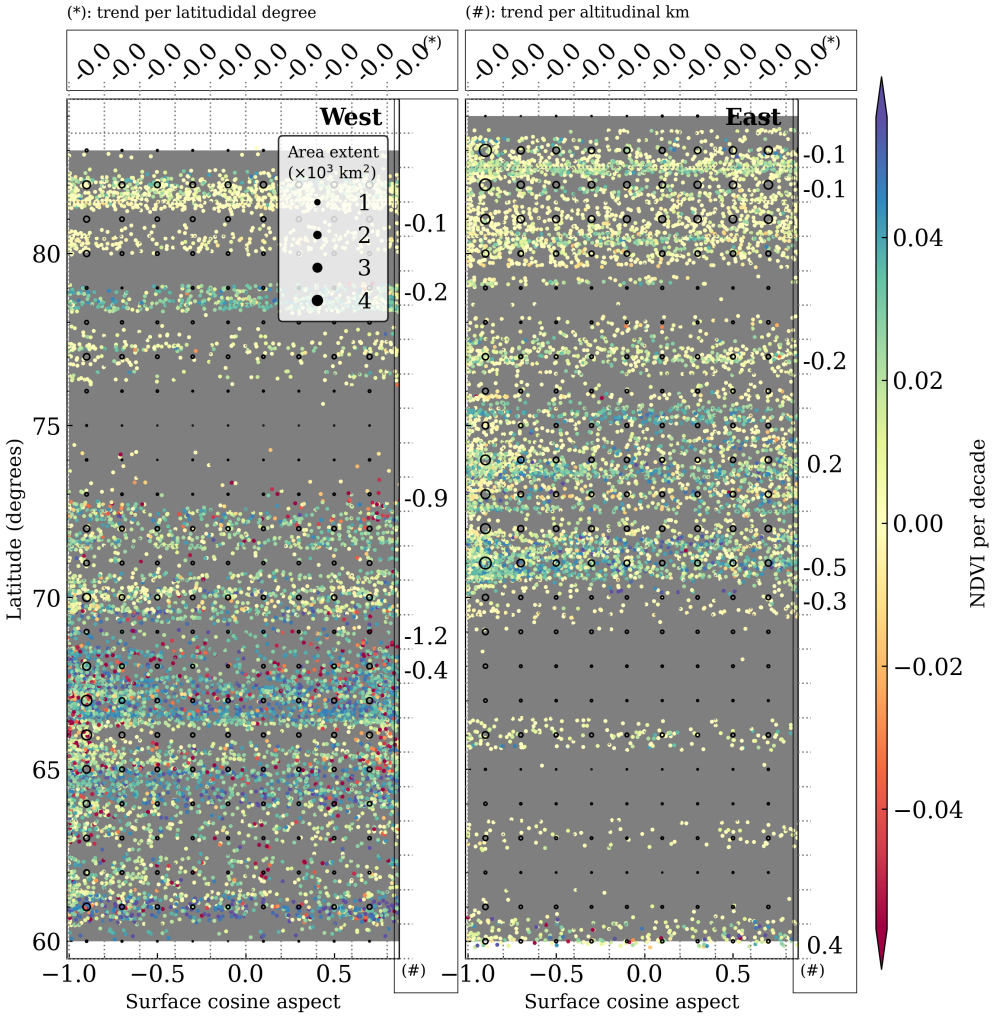

Figure S23. Significant trends for spectral greenness (in unitless per decade) in the ice-free part of West (left panel) and East (right panel) Greenland. The trend's cosine-aspect dependency (unitless) is binned in one degree of latitude and shown in vertical boxes marked with (#). The trend's latitudinal dependence (in unitless per latitudinal degree) is binned every 0.2 and shown in horizontal boxes marked with (*). The background grey shade displays the cosine-aspect extent of ice-free Greenland in the respective degree, and the black circles represent the area extent by 0.2 cosine-aspect and latitudinal bin. At least 50 pixels (approx. 312 km^2) are required within each bin to compute its regression, otherwise not displayed. Trends are considered significant for confidence levels in the Mann-Kendall trend test higher than 95%, with the null hypothesis that the slope is equal to zero.

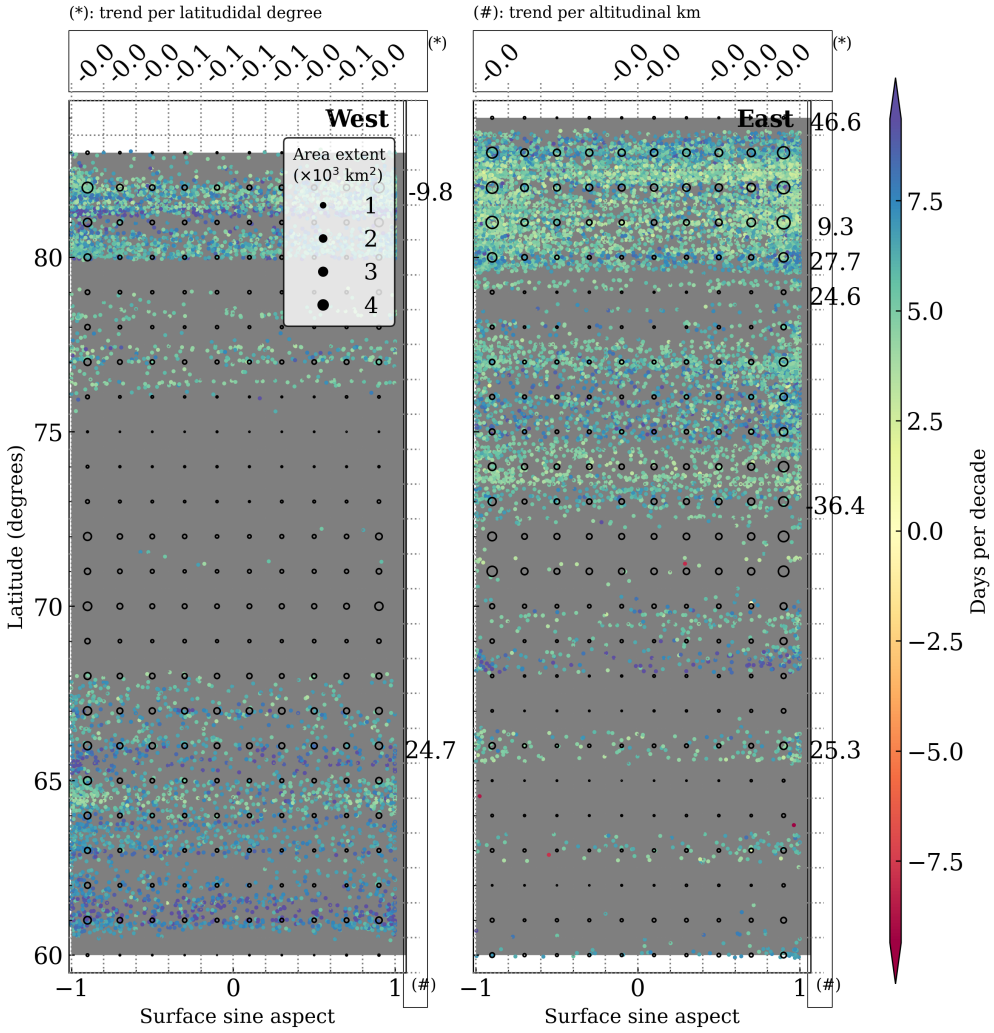

Figure S24. Significant trends for spectral greenness (in unitless per decade) in the ice-free part of West (left panel) and East (right panel) Greenland. The trend's sine-aspect dependency (unitless) is binned in one degree of latitude and shown in vertical boxes marked with (#). The trend's latitudinal dependence (in unitless per latitudinal degree) is binned every 0.2 and shown in horizontal boxes marked with (*). The background grey shade displays the sine-aspect extent of ice-free Greenland in the respective degree, and the black circles represent the area extent by 0.2 sine-aspect and latitudinal bin. At least 50 pixels (approx. 312 km^2) are required within each bin to compute its regression, otherwise not displayed. Trends are considered significant for confidence levels in the Mann-Kendall trend test higher than 95%, with the null hypothesis that the slope is equal to zero.